Membranes for organic solvent nanofiltration based on pre-assembled nanoparticles

Humera Siddique, Ludmila G. Peeva*, Konstantinos Stoikos**, George Pasparakis**,*

*Maria Vamvakaki**, Andrew G. Livingston*†*

* Department of Chemical Engineering and Chemical Technology, Imperial College London, Exhibition Road, London SW7 2AZ, UK

** Institute of Electronic Structure and Laser - Foundation for Research and Technology Hellas, 711 10 Heraklion, Greece

† a.livingston@imperial.ac.uk

Abstract

A new class of organic solvent nanofiltration (OSN) membranes has been fabricated by assembling nano-sized polymer particles with methacrylate moieties onto the surface of crosslinked polyimide ultrafiltration support membranes. Multiple layers of these nanoparticles create a separation film functionally similar to the top layer of an asymmetric OSN membrane. Nanoscale interstitial spaces formed between the particles serve as permeation channels. In principle, manipulating the size of the nanoparticles can be used to control the dimensions of the interstitial spaces through which permeation occurs. Two different sizes of nanoparticles - 120

and 300 nm - were used. As expected, membrane separation performance changed with the size of nanoparticles employed due to the changes in interstitial dimensions. Crosslinked polyimide ultrafiltration membranes prepared by phase inversion were coated with successive layers of nanoparticles by spin coating. After coating the nanoparticles were crosslinked by photo initiated free radical polymerization using ultraviolet light (365nm wavelength). In addition to the size of the nanoparticles, the separation performance was also manipulated by changing the thickness of the nanoparticle layer. Membranes were characterized using scanning electron microscopy. The nanofiltration performance of these membranes was evaluated in solvents such as acetone and toluene. The molecular weight cut-off (MWCO) of the membranes was from 200-1,000 $g.mol^{-1}$ depending upon the nanoparticle diameter and thickness of the nanoparticle layer. Thus membranes with graded nanoscale porosities were successfully fabricated from interconnected nanoparticles providing control over membrane permeation performance.

1. Introduction

Organic solvent nanofiltration (OSN) is gaining importance among both academic and industrial researchers[1, 2]. OSN is a technique for economic and efficient separation of molecules in the range of 200-1,000 $g.mol^{-1}$ which are dissolved in organic solvents. It has been successfully applied in a variety of chemical processes such as catalyst recovery, solvent recycling, chiral separations and ionic liquid separation[3-5]. The most widely studied and commercialized OSN membranes are asymmetric polymeric membranes prepared by the phase inversion technique. Polyimides (PI) are the most commonly used polymers for OSN due to their excellent thermal and chemical stability in organic solvents[6, 7].

It is believed that the separation performance of these PI membranes is determined by the dense top layer formed during phase inversion. The separation performance (flux and rejection) can be varied by changing the solvent/co-solvent ratio and polymer weight % in the dope solution[8]; however achieving a wide range of MWCO and perfect separation of molecules in a narrower range using this technology is still difficult and limits the use of OSN membranes in many important applications. Accurate control over the membrane structure at molecular level has so far proved challenging using phase inversion. Membranes prepared by phase inversion typically have wide distribution of pore sizes in the separation layer, and control over the number of pores is still difficult.

To overcome this problem there is a need for development of new methods for fabrication of OSN membranes with control of structure at a molecular level. To the best of our knowledge only a few studies are available on membrane fabrication using controlled building blocks to form permeation passages in a manipulated way[9-14]. In these studies colloidal latex polymer particles were deposited on micro porous polymer supports to get membranes in ultra and microfiltration ranges for aqueous applications. Such colloids can be packed in regular arrays in which the bulk porosity depends on the geometry and is independent of the size of the nanoparticles[12-14].

Another interesting self-assembled porous membrane is S-layer lattice from Bacillus species after depositing cell wall fragments on a microfiltration membrane, cross-linking the S-layer protein with glutaraldehyde, and degrading the peptidoglycan with lysozyme[15-18]. This ultrafiltration S-layer composite membrane showed sharp molecular weight cut off with a very steep curve.

In the last ten years block copolymers have gained attention due to the convenience of tuning size, shape and periodicity by changing their molecular parameters. Efforts have been made to

use block copolymers for fabricating nanostructured membranes[19]. Thomas et al. reviewed various methods to control block copolymer micro-domain structures in bulk states and in thin films[19]. Nanochannels can be created through processing of bicontinuous microdomain structure formed by microphase separation of a block copolymer. Continuous tortuous holes with nanometer scale diameters can be created by the selective degradation of one of the bicontinuous microdomain phases of micro-phase separated block copolymers[20]. Due to the structural versatility of block copolymers, they are used for analysis of permeation through polymeric materials. By correlating the permeability properties with the chemical structure of block copolymers, block copolymers can be modified towards high permeability[21].

Regular structures have also been obtained by introducing a melt of microphase separated polystyrene-block-polybutadiene into the pores of an anopore membrane via capillary action. Polymer cylindrical domains aligned parallel to the pore walls in the membrane[22]. Unfortunately, all the regular structures discussed above are still far from practical application in membranes.

This paper reports, for the first time, the use of preformed nanoparticles of narrow size distribution in the fabrication of solvent stable membranes in the nanofiltration range. Layers of these nanoparticles on a porous support form interstitial spaces with a narrow size distribution that reflects nanoparticle diameter. These spaces can serve as uniform pores which determine the nanofiltration performance of the membrane. Pore size is governed by the size of the nanoparticles. Fabrication of these membranes involves the formation of nanoparticles, depositing a layer of these on the top of a support membrane, and then stabilizing this layer by crosslinking. By creating a controlled nanostructure in the top layer of a nanofiltration membrane, we seek the power to tune molecular permeation properties.

This paper emphasises the fabrication of these membranes by using different sizes of nanoparticles, varying nanoparticle layer thickness, and evaluating the nanofiltration performance of the resulting membranes. Structural studies were undertaken using scanning electron microscopy.

2. Materials and methods

2.1 Materials

The monomers, *N*-isopropylacrylamide (NIPAM) and 2-(hydroxy) ethyl methacrylate (HEMA), the crosslinker *N, N'*-Methylenebis(acrylamide) (BIS), the stabilizer dodecyl sulfate sodium salt (SDS) and triethylamine (TEA) used for the microgel synthesis were purchased from Sigma-Aldrich (Germany). 2, 2'-Azobis (2-methylpropionitrile) (AIBN) and acryloyl chloride (AcCl) were obtained from Acros Organics and Fluka, respectively. The organic solvents used were of HPLC or analytical grade, and were purchased from Sigma-Aldrich (Germany). Milli-Q water (18.2 MΩ) was used in all experiments.

P84 polyimide was purchased from HP Polymer GmbH (Austria) and used without any pre-treatment. Organic solvents (all obtained from Sigma–Aldrich, UK) used to prepare the membranes and for filtration experiments were *N*, *N*-dimethylformamide (DMF), methanol, toluene, acetone and isopropanol (IPA). The crosslinker for the ultrafiltration support membranes was 1, 6-hexanediamine (HDA) purchased from Sigma–Aldrich (UK). Commercial membranes Starmem 122 (MWCO~220 $gmol^{-1}$), Puramem 280 (MWCO~280 $gmol^{-1}$) and S380 (MWCO~380 $gmol^{-1}$) (MWCO as provided by the supplier) were purchased from Evonik Membrane Extraction Technology Ltd (UK).

2.2 Methods

2.2.1 Nanoparticle synthesis

The PNIPAM-based microgel particles were synthesized by emulsion copolymerization of NIPAM and HEMA using BIS as the crosslinker. Polymerization took place in a 500 mL flask containing 200 mL Milli-Q water. Next, SDS (150 mg, 0.52 mmol) was added to the flask under stirring followed by the addition of BIS (339 mg, 2.2 mmol), NIPAM (8 g, 0.07 mol) and HEMA (1.5g, 11.5 mmol). The flask was sealed with a rubber septum and the reaction was purged with N_2 for 30 minutes, before the addition of the initiator, AIBN (80 mg, 0.487 mmol, and 0.7 wt% with respect to the monomers). Then the flask was placed in an oil bath at 70 ^{o}C under stirring and the reaction was allowed to proceed for 4 hours before exposing it to air to quench the polymerization. The nanoparticles were purified using an ultrafiltration unit (IVSS Vivacell) equipped with a 10,000 MWCO cellulose membrane to remove the stabilizer and any unreacted starting materials. The purification process was repeated 2-3 times using fresh water before collecting the particles from the ultrafiltration unit as a dense paste (ca. 50 wt% polymer content).

2.2.2 Particle acrylation

The P(NIPAM-HEMA) nanoparticles were modified using acryloyl chloride to introduce polymerizable vinyl moieties on their surfaces. 3 g of nanoparticles were diluted with THF (ca. 10 mL) and added to a dialysis membrane for solvent exchange against excess THF (700 mL) for 2 days during which time the solvent was regularly replaced with fresh THF. Next, the nanoparticles (3 g in 30 mL THF) were transferred to a 100 mL round-bottom flask, and triethylamine (0.043 moles, ca. 1.2 eq. with respect to the HEMA moles) was added. The flask was sealed with a rubber septum and placed in a thermostatted bath at 0 ^{o}C under magnetic stirring. Acryloyl chloride (390mg, 4.3mmol, 1 eq. with respect to the HEMA moles) was added dropwise using a glass needle. After 2 hours, the reaction was stopped and the mixture was dialyzed against water (1 L) for 2 days to remove the triethylammonium chloride salt formed and

any unreacted starting materials. The purified nanoparticle suspension was stored in water at 4 ^{o}C for further use.

2.2.3 Ultrafiltration membrane preparation

Dope solution was prepared by adding 22 wt% PI to DMF at room temperature. Following polymer dissolution the dope solution was left for 3 hours to remove air bubbles. The dope solution was then used to cast 250 µm thick viscous films on a polyester (PET) non-woven backing material (Kavon filters, USA), using an adjustable casting knife (Elcometer 3700) on a bench casting machine (Braive Instruments). An evaporation period of 20 seconds was allowed before immersion in a water coagulation bath at room temperature. Residual water was removed from the membrane by placing it in IPA for one hour. The membrane was transferred from IPA to the crosslinking solution (HDA in IPA). Following this, the membrane was rinsed with IPA to remove residual HDA. The membrane was finally subjected to the conditioning step in which it was kept for four hours in a conditioning solution comprising polyethylene glycol (PEG) 400/IPA (60/40 wt.%, respectively). The membrane was then air dried to remove solvent.

2.2.4 Nanoparticles coating

The nanoparticles were suspended in methanol (5 wt %). 1 wt% of UV initiator (55, 66-Tetrahydroxy-3, 3, 3', 3'-tetramethyl-1, 1'-spirobisindane) was also added to the nanoparticles suspension. The ultrafiltration membrane described above (sec 2.2.3) was coated with nanoparticles by spin coating. For each coat 0.5 ml of nanoparticles suspension was used and spread over the ultrafiltration membrane at 500 revolutions per minute (rpm) for the first 10 seconds and 2000 rpm for a further 50 seconds and then dried for 30 seconds before the next coat.

2.2.5 Crosslinking of nanoparticles

After the coating the membrane was irradiated under UV light (Black ray B-100 high intensity UV lamp, power 100 watts and wavelength 365 nm) for 3 hours to crosslink the nanoparticles by radical polymerization (conversion of methylmethacrylate to polymethylmethacrylate). The membrane was then used without any further treatment. A summary of the membranes prepared in this way is presented in Table 1.

Table1. Membrane preparation conditions

Membrane code	**Nanoparticle diameter (nm)**	**Nanoparticle coats applied**	**Concentration of nanoparticles in suspension**
M1	.....	0 (UF crosslinked support)	.....
M2	120	1	5wt%
M3	120	2	5wt%
M4	120	3	5wt%
M5	300	1	5wt%
M6	300	2	5wt%
M7	300	3	5wt%
M8	300/120	2/2	5wt%/5wt%
M9	300	1	2.5wt%
M10	300	2	2.5wt%
M11	300	3	2.5wt%

2.3 Nanoparticles characterization

2.3.1 Scanning electron microscopy (SEM)

SEM images were recorded using JEOL JSM-840 (large particles) and a field emission JSM-7000F (small particles) microscopes at electron acceleration voltages of 10 and 15 kV,

respectively. Samples were prepared by diluting an aliquot of the stock nanoparticle suspension in THF (0.01 wt %). A drop of the sample (20 μL) was deposited onto a glass slide and left to dry overnight. The sample was sputter-coated with Au (10 nm thickness) before imaging.

2.3.2 Dynamic light scattering (DLS)

Samples were prepared by diluting an aliquot of the stock nanoparticle suspension in water (0.1 wt%, 5 mL). Before measurement, the samples were filtered using a 5 μm pore size syringe filter and were transferred to a glass cuvette. A 3D LS Spectrometer from LS Instruments with a HeNe laser operating at λ=632.8 nm was used and all measurements were performed at 20^{o} C. The samples were measured for 600 seconds at each scattering angle.

A single stretched exponential decay (KWW type) was used to fit the intensity autocorrelation functions

$$C(q.t) = A.\exp\left(-\frac{t}{\tau}\right)^2 \quad (1)$$

Where A is the amplitude, τ the relaxation time and q the stretching factor. The rate Γ for each angle was calculated as $\Gamma = \frac{1}{\tau}$. From equation $\Gamma = D.q^2$ the diffusion coefficient D was obtained from the slope of the linear fit of the graph of Γ versus q^2. Finally, the diffusion coefficient and the hydrodynamic radius R_h are related by the Stokes Einstein equation:

$$R_h = \frac{k_B T}{6\pi\eta D} \quad (2)$$

Where η is the viscosity of the solvent, k_B is the Boltzmann constant and T is the temperature of the sample.

2.3.3 Infrared spectroscopy (ATR-FTIR)

ATR-FTIR spectra of dried samples were recorded on a Thermo-Electron Nicolet 6700 FTIR optical spectrometer at a resolution of 2 cm^{-1}.

2.4 Membrane characterization

2.4.1 Scanning electron microscopy (SEM)

Images of cross-sectional areas of the membranes were obtained using SEM (Leo 1525 field emission scanning electron microscope, FESEM). After removing the backing material, membranes were snapped in liquid nitrogen, mounted onto SEM stubs, and coated with chromium using a chromium sputter coater (Emitech K575X). Applied SEM conditions were: a 6.5mm working distance and an in lens detector with an excitation voltage of 5 kV.

2.4.2 Nanofiltration experiments

All nanofiltration experiments were carried out in a continuous cross-flow system, at 30×10^5 Pa with toluene or acetone as a solvent at 27°C and using feed flow rate of 80-100 $L.h^{-1}$. Permeate samples for flux measurements were collected at intervals of 1 hour, and samples for rejection evaluations were taken after steady permeate flux was achieved. MWCO curves were obtained using a standard test solution composed of a homologous series of styrene oligomers dissolved in toluene and acetone. The styrene oligomer mixture contained 1 $g.L^{-1}$ each of PS 580 and PS 1050 (Polymer Labs, UK), and 0.01 $g.L^{-1}$ of methylstyrene dimer (Sigma–Aldrich, UK). Concentrations of styrene oligomers in permeate samples were analyzed using an Agilent HPLC system with a UV/vis detector set at a wavelength of 264 nm. Separation was accomplished using an ACE 5-C18-300 column (Advanced Chromatography Technologies, ACT, UK). A mobile phase comprising 35 volume% analytical grade water and 65 volume% tetrahydrofuran with 0.1 volume% triflouroacetic acid was used[23]. Solvent flux (J) was determined by measuring the volume of permeate (V) per unit area (A) per unit time (t) according to the following equation:

$$J = \frac{V}{At} \tag{3}$$

Flux decrease of the membranes (D_f) was calculated according to the following equation:

$$D_f = \left(\frac{(J_i - J_s)}{J_i}\right) \times 100\% \quad (4)$$

Where J_i is the initial flux and J_s the flux at steady state (achieved when two flux measurements within a 1-hour interval showed the same value within ±2 Lm^{-2} h^{-1}). Rejection (R_i) of styrene oligomers was evaluated applying Eq. (5) in which C_{Pi} and C_{Fi} correspond to styrene oligomers concentration in permeate and in feed solution, respectively.

$$R_i = \left(1 - \frac{C_{Pi}}{C_{Fi}}\right) \times 100\% \quad (5)$$

The corresponding MWCO curves were obtained from a plot of the rejection of styrene oligomers versus their molecular weight.

2.4.3 Calculation of nanoparticle layer thickness

Physical thickness of membranes before and after coating with nanoparticles was measured with a micrometer (Mitutoyo Japan, range 0.0001μm). The number of nanoparticle layers was calculated as follows:

Considering the nanoparticle as a sphere, the volume of one nanoparticle (V_n) was calculated as:

$$V_n = \frac{4(\pi {r_n}^3)}{3} \quad (6)$$

Cross sectional area of one nanoparticle (A_n) was calculated as

$$A_n = \pi {r_n}^2 \quad (7)$$

Considering the nanoparticles as closely packed spheres the total number of nanoparticles in one layer (N_n) was calculated from equation 8 based on the assumption that if a perimeter of a single layer of nanoparticles is projected onto a two dimensional image, the result is a collection of circles on a surface and the area not covered by the circles is 10% of the total area covered[24]:

$$N_n = \frac{A_m}{A_n} \times 90\% \quad (8)$$

Where A_m is surface area of membrane.

The total volume (V) of nanoparticles coated on the membrane was calculated as

$$V = \frac{w}{\rho_n} \tag{9}$$

Where w is the weight increase in the membrane after coating with nanoparticles and ρ_n is the density of nanoparticles. The total number of nanoparticles (N_{total}) coated can be calculated as:

$$N_{total} = \frac{V}{V_n} \tag{10}$$

Finally the number of nanoparticles layers (L_n) was calculated as:

$$L_n = \frac{N_{total}}{N_n} \tag{11}$$

The nanoparticle layer thickness (T) can be calculated as (packing density of 0.7408 is known to be the densest possible packing of equal spheres[25]).

$$T = \frac{V}{A_m \times 0.7408} \tag{12}$$

3. Results and discussion

3.1 Nanoparticle characterization

The P(NIPAM-HEMA) microgel nanoparticles were synthesized by emulsion copolymerization in aqueous media. Owing to its sharp lower critical solution temperature at ca. 32 ^{o}C, PNIPAM core seeds were rapidly formed soon after polymerization initiation at 70 ^{o}C, accompanied by the formation of hydrophilic PHEMA chains around the NIPAM-based precursors. Therefore, a core-shell topology was obtained in a one-pot type reaction (Figure 1A). The size of the microgels was controlled by adjusting the overall monomer concentration, the NIPAM/HEMA mole ratio and the surfactant concentration in the polymerization mixture.

Microgels of two different sizes (120 and 300 nm in diameter) were used throughout the study for the coating of the membranes' surfaces.

In order to facilitate the interparticle crosslinking onto the surfaces of the membranes, the hydroxyl-rich microgel shells were modified with acrylate moieties by esterification with acryloyl chloride (Figure 1B).

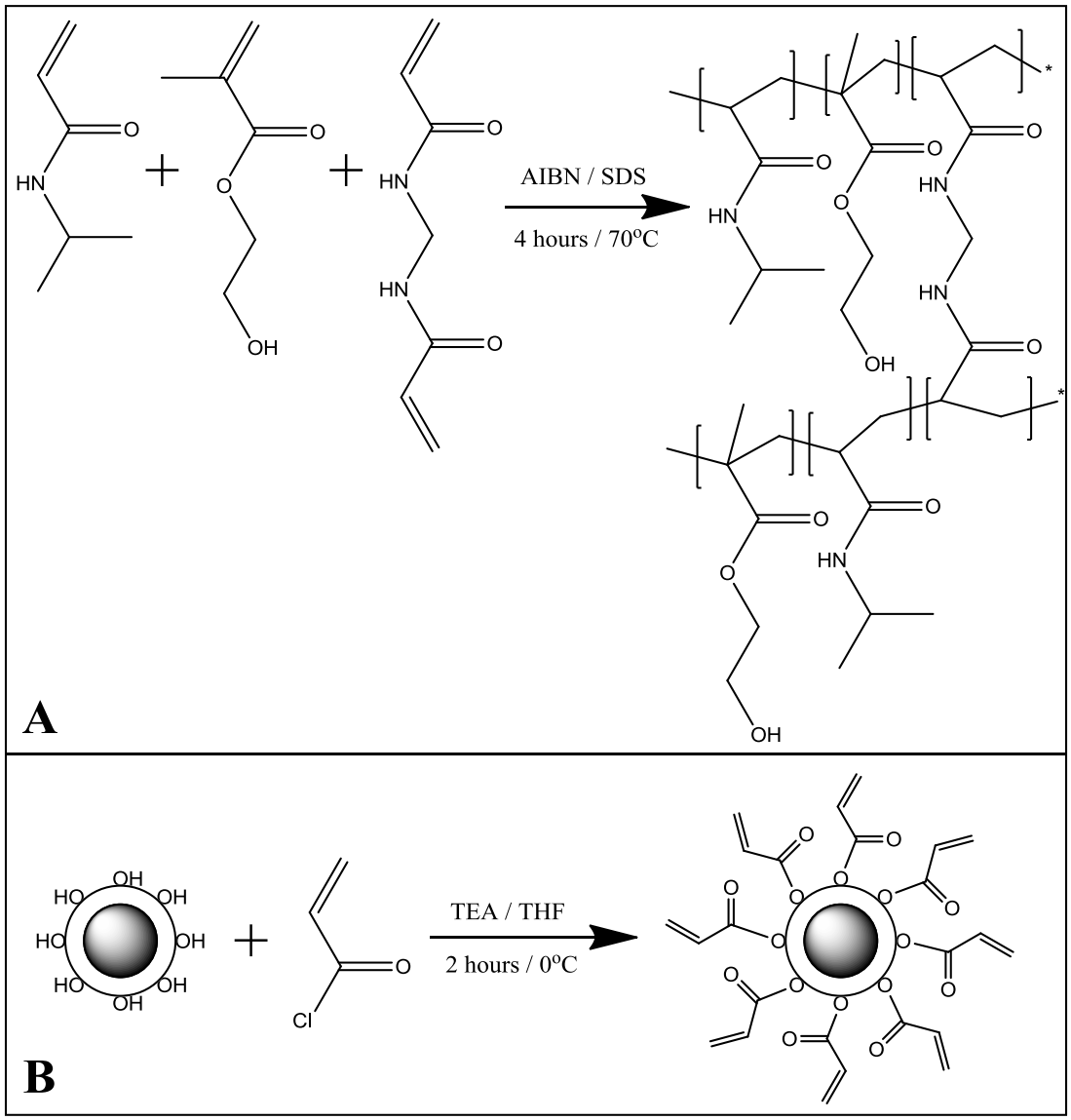

Figure 1. A) Schematic representation of the polymerization process followed for the synthesis of the crosslinked P (NIPAM-HEMA) particles; B) Schematic representation of the acrylation process employed to introduce crosslinkable vinyl groups on the surface of the particles.

The size of the particles was determined by DLS measurements. The intensity autocorrelation functions at different scattering angles were found to be dominated by a single process, which is indicative of a single particle population (Figure 2A). The diffusion coefficient (D) was

calculated from the wavevector dependence of the rate of this process (Figure 2B) which corresponds to a hydrodynamic radius of R_h = 148 nm for the large particles. A similar size (R_h = 141 nm) was found for the particles after the acrylation process, signifying that the mild conditions used for the acrylation reaction do not affect the particle size. Similarly, for the smaller particles (Figure 3) the hydrodynamic radius was R_h = 60 nm and R_h = 61nm before and after the acrylation reaction, respectively (Figure 3B).

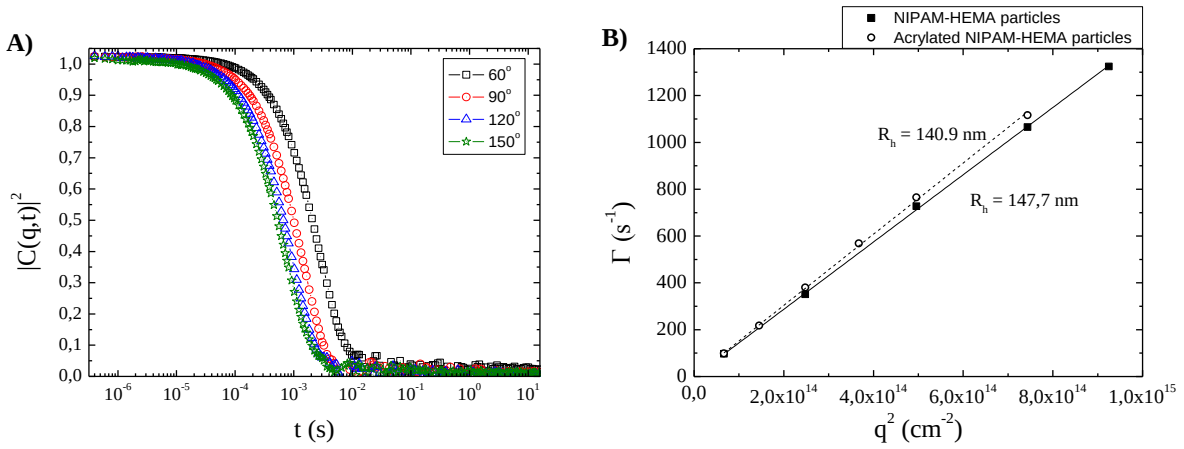

Figure 2. A) Intensity autocorrelation functions for the large P(NIPAM-HEMA) particles' dispersion at scattering angles 60°, 90°, 120° and 150°. B) Rate as a function of q^2 for the P(NIPAM-HEMA) particles and the acrylated P(NIPAM-HEMA) particles. The lines are linear fits to the data.

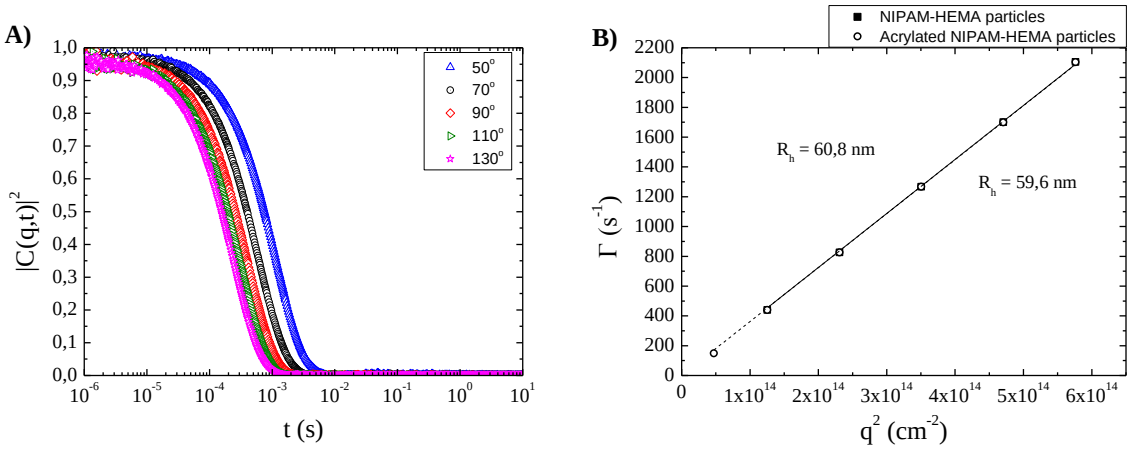

Figure 3. A) Intensity autocorrelation functions for the small P(NIPAM-HEMA) particles' dispersion at scattering angles 30°, 50°, 70°, 90°, 110° and 130°. B) Rate as a function of q^2 for the P(NIPAM-HEMA) particles and the acrylated P(NIPAM-HEMA) particles. The lines are linear fits to the data.

The morphology and the size of the P (NIPAM-HEMA) particles were also investigated by SEM (Figure 4). Particles of a spherical shape and a uniform size distribution with diameter $\langle D_{SEM} \rangle$ = 125 nm and $\langle D_{SEM} \rangle$ = 120 nm before and after acrylation, respectively were observed for the smaller particles (Figure 4, right). Overall, there is a good agreement between the particle sizes found by SEM and those calculated from the DLS measurements. The slightly smaller sizes obtained by SEM were attributed to the drying of the particles on the glass substrate which resulted in the partial collapse of the polymer network.

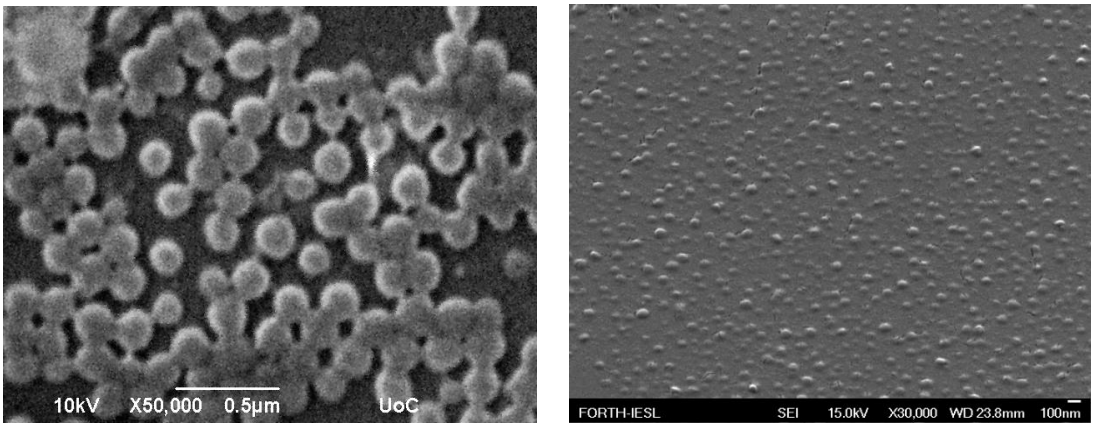

Figure 4. Typical SEM images of the 300 nm (left) and 120 nm (right) microgels.

FTIR spectroscopy was used to verify the successful acrylation of the microgel particles by the presence of the vinyl bond vibration band. Figure 5B shows the FTIR spectrum of the acrylated particles, where the characteristic peak of the vinyl bond[26-28] at 800 cm^{-1}, which is absent in the spectrum of the precursor particles (Figure 5A), can be clearly seen. Besides, the characteristic ester and amide bands at 1500-1800 cm^{-1}, present in the spectra of the particles both before and after acrylation, verify the successful incorporation of the co-monomers and the amido based crosslinker in the particles. Although the FTIR spectra confirm the successful surface modification of the particles, they do not allow quantification of the overall yield of the acrylation. It is expected though that the esterification reaction used should exceed 80% yield.

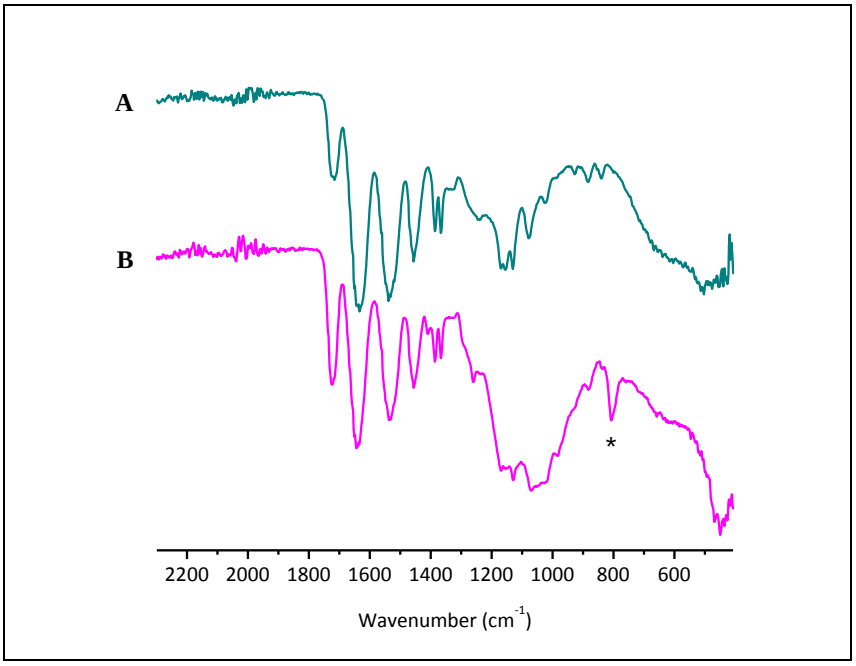

Figure 5. ATR-FTIR spectra of A) the P (NIPAM-HEMA) precursor particles and B) the acrylated P(NIPAM-HEMA) particles

3.2 Nanoparticle coated membrane characterization

3.2.1 Scanning electron microscopy of the membranes

SEM images were taken of membrane cross sections at three different magnifications. Images were taken to calculate the nanoparticle layer thickness and the distribution of the nanoparticles on the ultrafiltration support. Figures 6 and 7 show the resulting asymmetric composite membranes with two different types of pore; a base of broadly dispersed irregular pores, and a top layer of narrow pores situated between uniformly packed spheres. The evenly spaced morphology is formed from the spin coating by evaporation of solvent. By comparing Figure 6 with Figure 7 it is clear that the nanoparticle layer thickness increases with larger diameter nanoparticles. The mean pore size of the membrane changes with the change in thickness of the separating layer (nanofiltration results presented later confirm this trend). From the SEM images

some nanoparticle deformation is observed, which is more explicit for the larger nanoparticles (see the discussion in section 3.2.3). Another interesting observation from the SEM images is that the nanoparticles apparently penetrated into the pores of the ultrafiltration membranes. It seems likely that during the first coat, before formation of the particle layer, some particles penetrated through the bigger pores - a wide range of pore sizes are present in the ultrafiltration support.

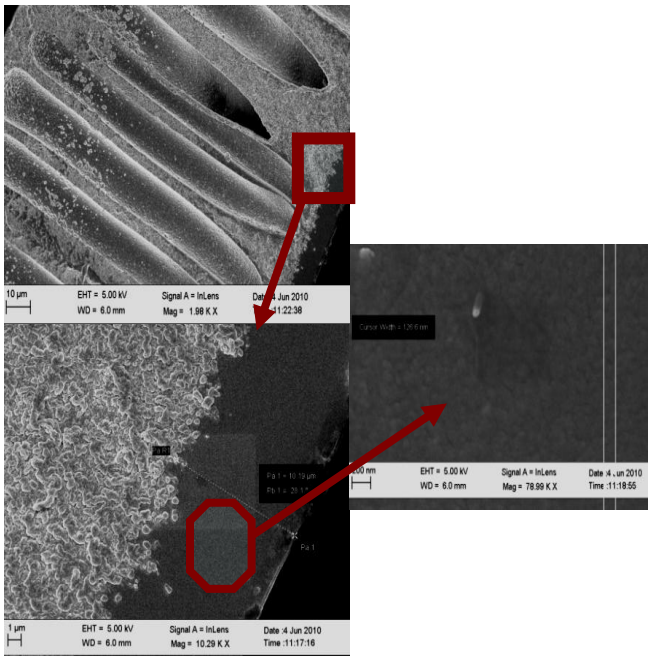

Figure 6. SEM images of a cross sectional area of polymer ultrafiltration support, with three coats of 120 nm diameter nanoparticles at three different magnifications 1.98KX, 10.29KX and 78.99 KX.

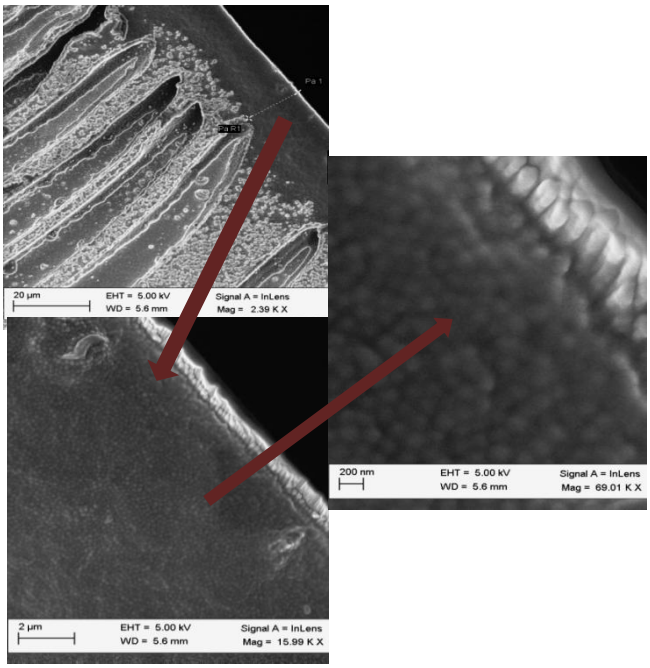

Figure 7. SEM images of a cross sectional area of polymer ultrafiltration support with two coats of 300 nm diameter nanoparticles at three different magnifications 2.39KX, 15.99 KX and 69.01 KX.

3.2.2 Nanoparticle layer thickness and calculation of the number of nanoparticle layers in the film

The nanoparticle layer thickness coated on the membrane was measured in two ways, and then compared with theoretical calculations based on closely packed spheres. All measurements are the average of 5 different points on 3 different disks. Thickness measured by SEM and micro meter showed similar values, but the calculated thicknesses were higher than the measured ones. Based on the results shown in Table 2 it seems that in the first coat not all nanoparticles were deposited on the surface. Some nanoparticles penetrated into the porous support (as confirmed by SEM images). The theoretically calculated thickness was based on the weight increase of the membrane after coating and did not take into account the particles in the porous support, which

contributes to the calculated thickness being higher than the measured values. In addition particle deformation could be also responsible for this difference as will be discussed in the following section. As could be expected the thickness also increased with the increase of the size of nanoparticle. The nanoparticle layer thickness decreased for the same size of nanoparticle with same number of coats but with lower concentration. (Table 2, M9-M11) By lowering the concentration, the total number of nanoparticles deposited was smaller, making the nanoparticle layer thinner. It could be expected that a lower number of nanoparticles will result in a packing which deviates considerably from the ideal case of closely packed spheres, and consequently a wider pore size distribution due to defects in the packing. This hypothesis was confirmed by membrane separation performance.

Table 2. Dimensions of the nanoparticles layers

Membrane code	No of layers	Thickness calculated (µm)	Thickness measured micrometer (µm)	Thickness SEM measured (µm)
M2	20	2.2	0.9	0.76
M3	113	12.1	7.5	6.9
M4	282	30.4	17.5	15.3
M5	7	2.5	1.1	1.2
M6	55	18.1	11.4	12.5
M7	123	40.6	21.3	23.5
M8	.....	28.2	12.1	14.3
M9	4	2.1	1.1	0.9
M10	29	12.0	7.5	7.6
M11	67	26.7	15.1	14.2

3.2.3 Nanofiltration experiments

A continuous crossflow rig was used to perform nanofiltration experiments. Rejection of styrene oligomers was plotted against their molecular weights to determine the MWCO of the membranes coated with nanoparticles. All the results shown in Figures 8-15 were repeated three times for three different batches of membranes and these results were reproducible with coefficient of variation of 10% for both flux and rejection.

According to the size of nanoparticles, membranes coated with them were not expected to separate molecules in the nanofiltration range (9-23nm estimated pore size, from Eq. 17, section 3.2.4). However, the rejection of styrene oligomers indicated that separation in the nanofiltration range did in fact occur. This phenomenon was investigated in the light of nanoparticle layer formation. Formation of the nanoparticle film arises from the compaction, deformation, cohesion and polymer chain interdiffusion of individual particles. The particles are held apart by electrostatic or steric forces resulting from the polymer chain end groups. It is postulated that the particle layer is formed in three steps. The first step is evaporation of solvent and particle concentration and ordering. The second step is particle deformation, and the third step is polymer chain diffusion across the polymer boundaries[29-31].

Several factors affect the layer formation in this three stage process. Important factors are particle size, layer formation temperature, solvent concentration, time and drying environment[29]. The most important factor among these is the particle size. If the size of the particle is small then particles will pack and order quickly in more compact form in the first stage, the degree of deformation will be small in the next stage, and a more regular structure will be obtained. With larger particles, the interstitial space will be bigger in the first stage, with less organization of the particles, so deformation will be high in the second stage[32]. Our particles were 120 and 300nm in

size. Both sizes of nanoparticles could deform, however according to the above mechanism a higher degree of deformation is expected with the 300 nm nanoparticles. Although the SEM pictures do not allow easy detection, some indication of particle deformation can be observed in Figs. 6 and 7 if compared to their original shape (see Fig. 4). In addition, the measured particle layer thicknesses are considerably smaller than those theoretically calculated based on closely packed uniform spheres ones (Table 2). We speculate that the particle deformation could be responsible for membrane separation performance in the nanofiltration range. Furthermore P(NIPAM) is well known for its interchangeable properties and ability to "switch" from a hydrophilic to hydrophobic structure (from swollen to non-swollen state) and vice versa. Typically this behavior has been observed in response to temperature stimuli (when lower critical temperature has been passed) in aqueous solutions[33], however it could be possible that similar phenomena may occur in response to organic solvents. We did not find sufficient information in the literature on the material response to organic solvents and under pressure, and we are not sure whether the transport through the nanoparticles layer occurs solely through interstitial spaces between the particles or whether some transport is through the nanoparticles themselves. Our hypothesis is that the polystyrenes transport occurs through the interstitial spaces while the solvent permeates via both interstitial spaces (convective flow) and also through the nanaparticles themselves (diffusive flow). This hypothesis is supported by the findings of Cussler who discovered that when the P(NIPAM) gel swells, large solutes such as macromolecules will be excluded from entering the gel pores by steric hindrance and small solutes will freely penetrate the network[33].

The effect of the coating thickness of nanoparticles is shown in Figure 8. As the thickness of the top layer increases, so does the rejection because the pore size distribution becomes narrower

as there are less coating defects and the resistance to flow increases. Increasing size of the nanoparticles results in a more open top layer structure and higher MWCO. This effect can be observed in Figure 9, which compares separation properties (MWCO) of membranes formed from nanoparticles with different diameters, and comparable nanoparticle layer thickness. As the size of nanoparticles is increased, the interstitial space between the particles increases and hence the membrane becomes looser. Figure 10 (a) & (b) shows a decrease in solvent flux with increased thickness of nanoparticle layer (thickness data in Table 2), because the resistance of the nanoparticle layer increases with thickness.

Figure 11 shows the performance of multi-particle layers of different sized particles. Membranes were developed by coating first with particles of larger diameter, and then with smaller particles to decrease the mean pore size. As can be seen in Table 3 the membrane prepared in this way is tighter (MWCO 220), most likely due to the tighter packing of nanoparticles and patching of layer defects.

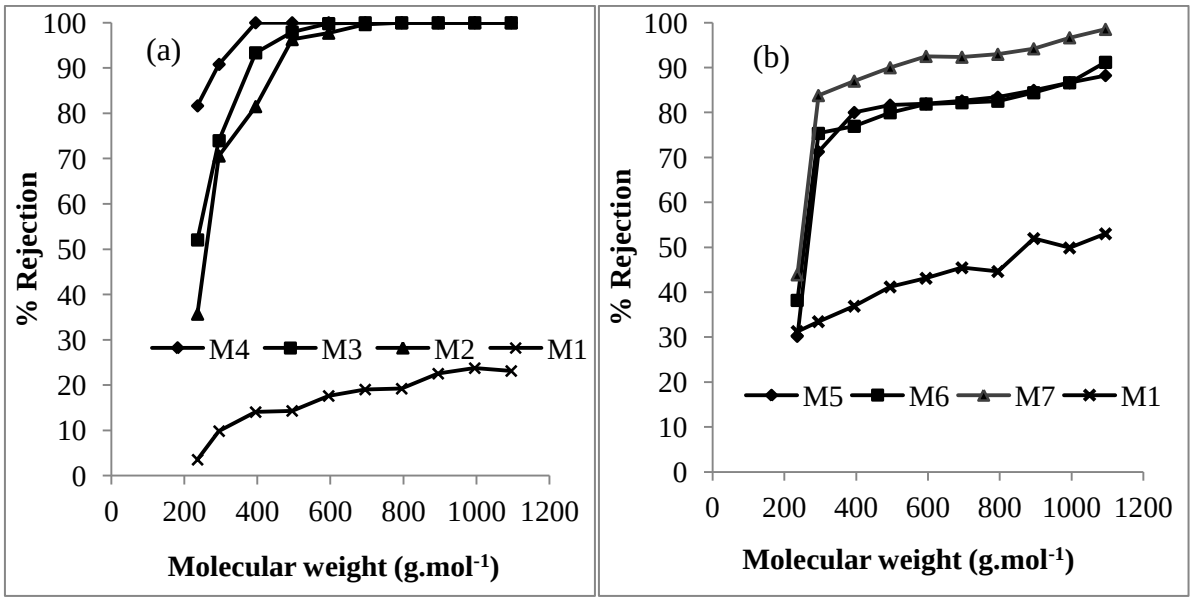

Figure 8. Rejection performances of nanoparticle membranes with respect to the number of coats (nanoparticle layer thicknesses respectively see Table 2) of (a) 120nm (b) 300 nm sized nanoparticles at 30 bar in PS/toluene solution and 27˚C

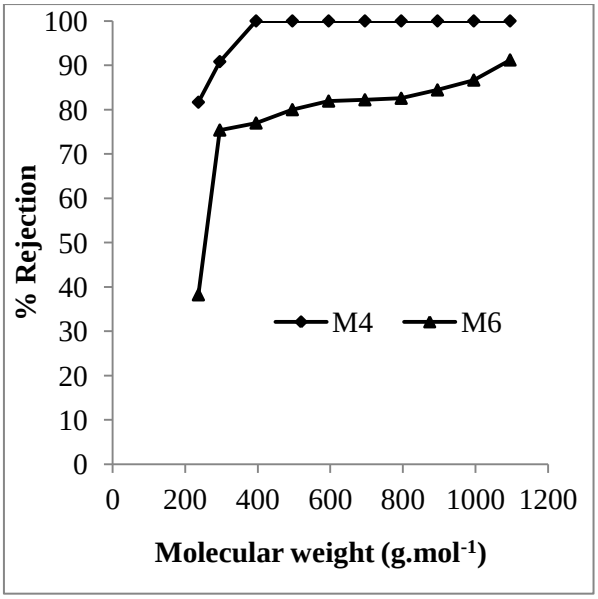

Figure 9. Rejection performances of nanoparticle membranes with respect to the size of nanoparticles (120 nm, 300 nm) at 30 bar in PS/toluene solution and 27˚C

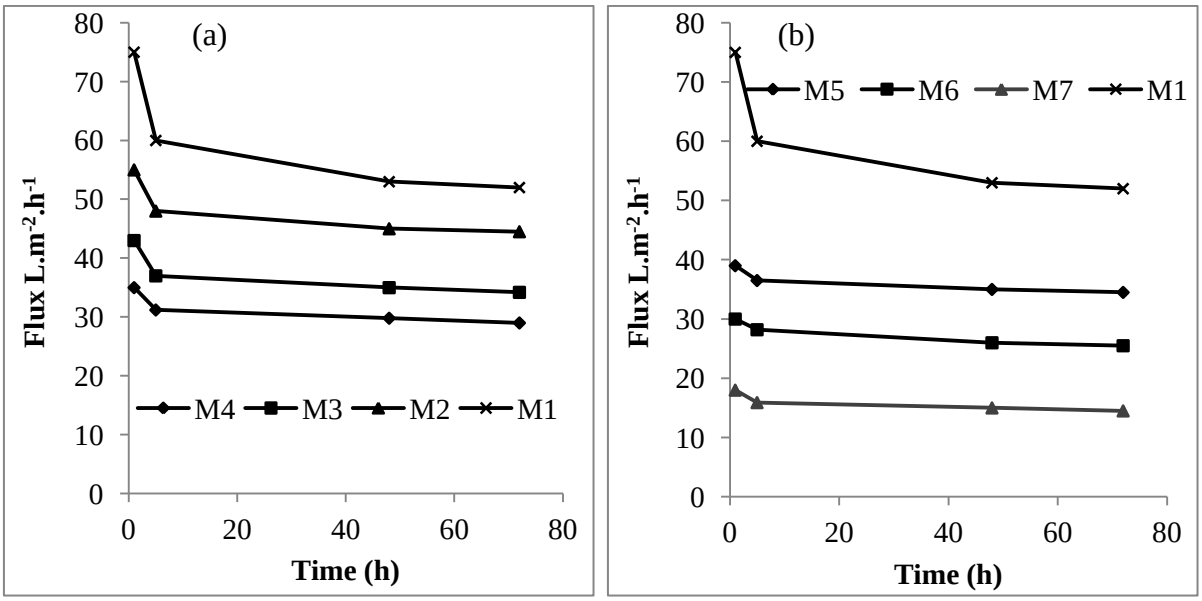

Figure 10. Permeate fluxes of nanoparticle membranes with respect to number of coats of (a) 120 nm (b) 300 nm sized particles at 30 bar and 27˚C in PS/toluene solution

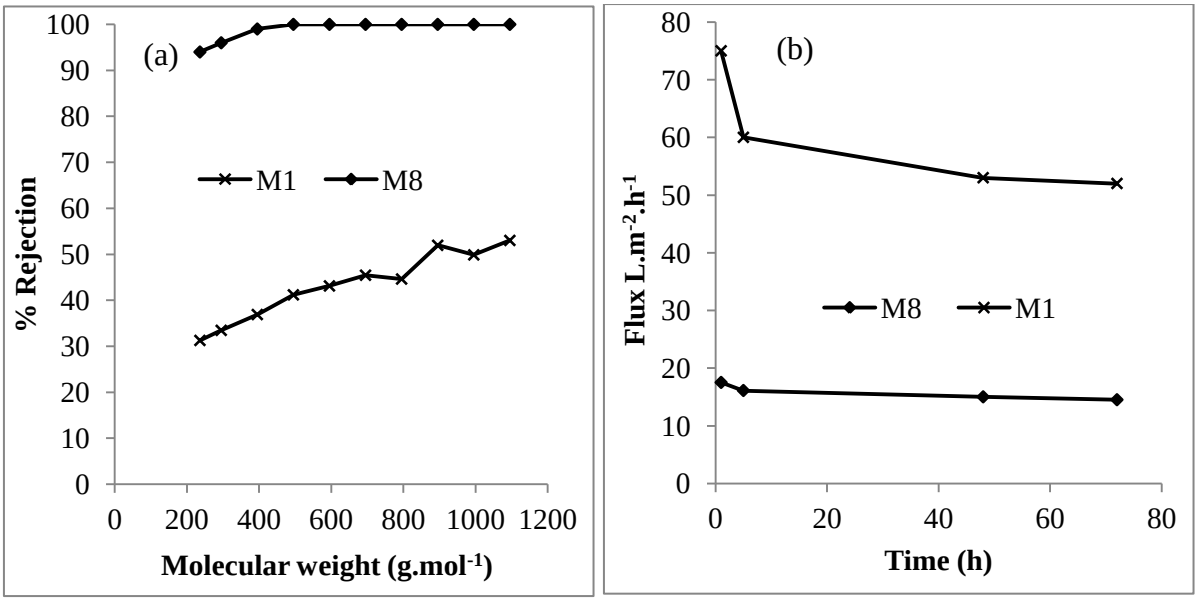

Figure 11. (a) Rejection performance (b) permeate flux of nanoparticle membranes with 2 coats of 300 nm sized particles and 2 coats of 120 nm sized particles at 30bar and 27˚C in PS/toluene solution

Figure 12 shows the effect of the concentration of nanoparticles on the membrane performance. It is clear from this figure that by decreasing the concentration of nanoparticles a more open membrane is obtained. One reason is the reduced thickness of the nanoparticle coat (Table 2), and most probably the presence of defects in the membranes with lower concentration.

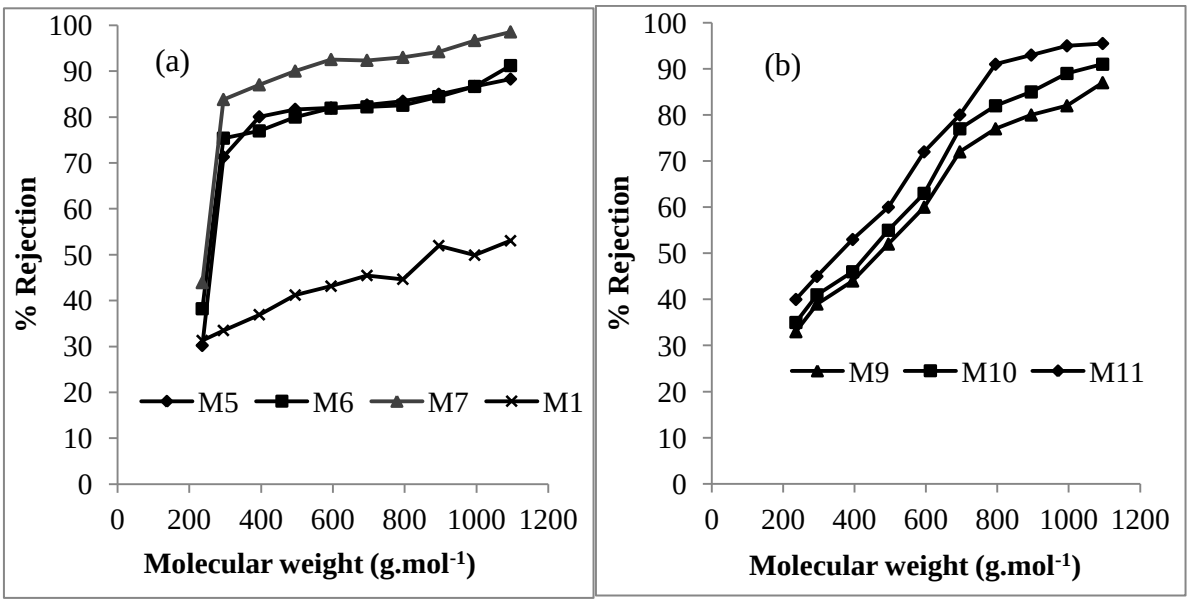

Figure 12. Rejection performances of nanoparticle membranes with respect to concentration of nanoparticles (a) 5 wt% nanoparticle solution (b) 2.5 wt% nanoparticle solution (300 nm) at 30 bar in PS/toluene solution and 27˚C

Figure 13 provides a comparison between nanoparticle coated membranes and the commercial OSN membranes Starmem 122, Puramem 280 and S380. It is clear that the membrane coated with nanoparticles shows better rejection performance (it is the tightest) and more resistance against compaction compared to these commercial membranes due to its more rigid regular structure. Although the initial flux is lower for the nanoparticle coated membrane, at steady state

there is no significant difference between the commercial membranes and the nanoparticle membrane when they are within the same MWCO range.

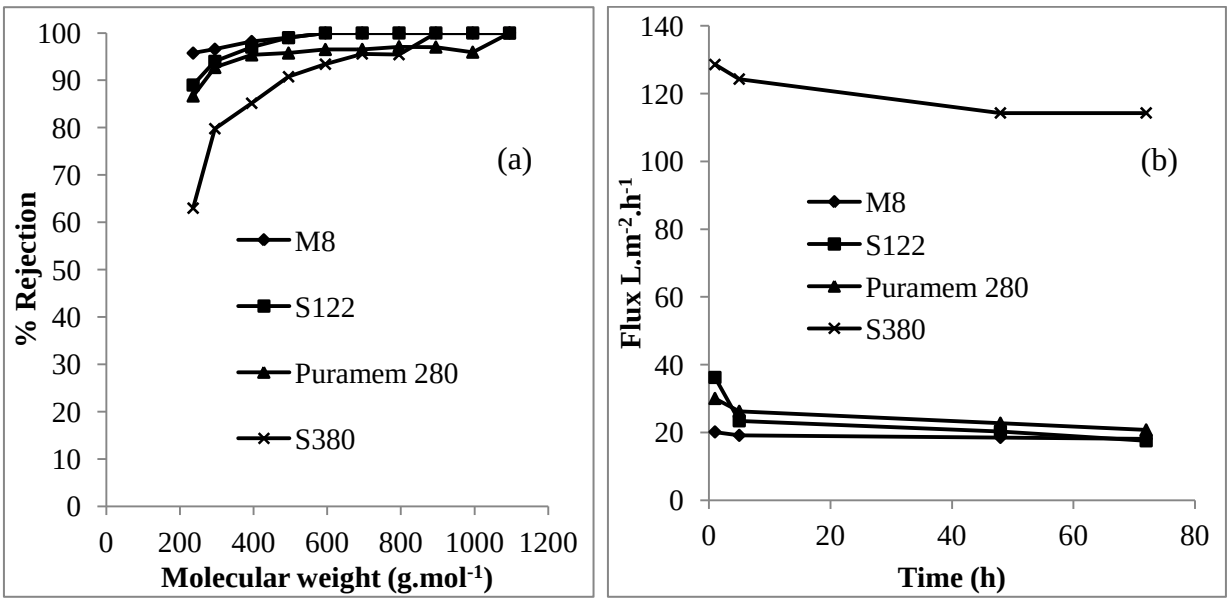

Figure 13. (a) Rejection performance (b) permeate flux of nanoparticle membrane with 2 coats of 300 nm sized particles and 2 coats of 120 nm sized particles and commercial membranes Starmem 122, Puramem 280 and S380 at 30bar and 27˚C in PS/toluene solution

The nanoparticle coated membranes were also investigated at lower pressure (10 bar, Figures 14 and 15) to evaluate the separation performance and nanoparticle layer stability, since it is possible that at lower pressure the nanoparticles could be more easily eluted from the membrane surface. The rejections were the same as at 30 bar pressure but as expected the fluxes were lower. The separation performance and flux remained stable during the test suggesting that the nanoparticle layer is not affected.

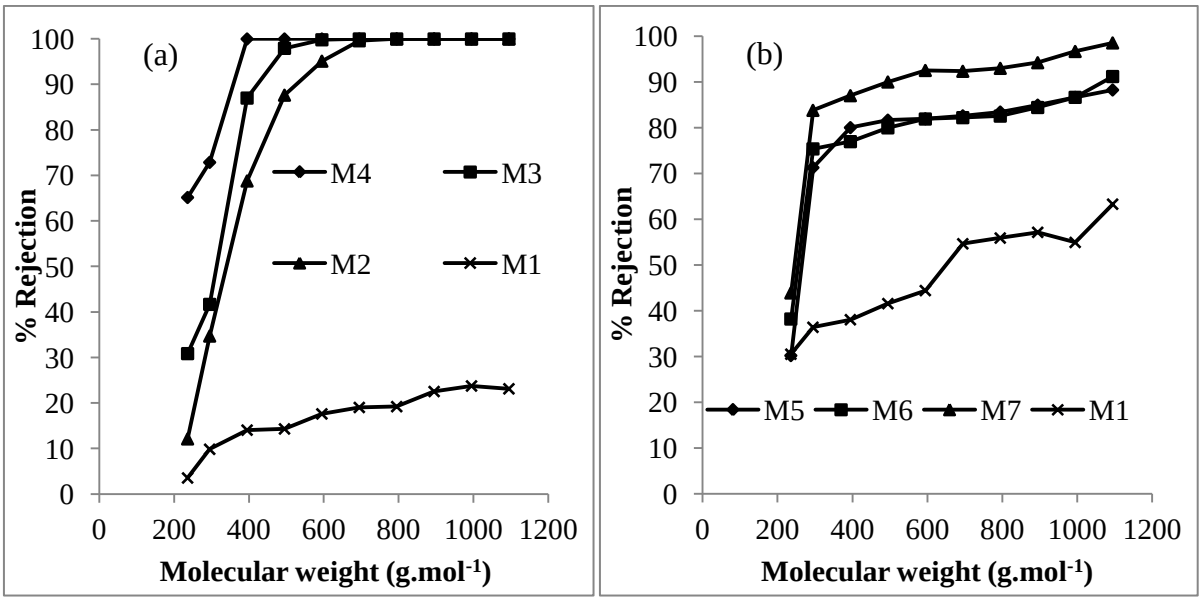

Figure 14. Rejection performances of nanoparticle membranes with respect to the number of coats (nanoparticles layer thicknesses respectively see Table 2) of (a) 120nm (b) 300 nm sized nanoparticles at 10 bar in PS/toluene solution and 27˚C

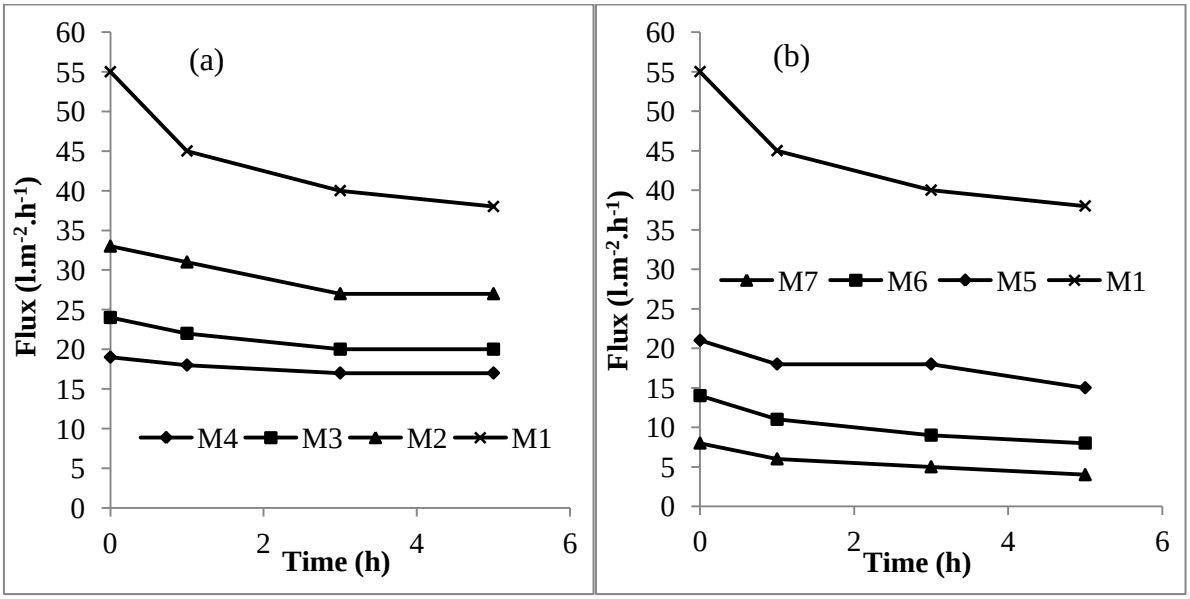

Figure 15. Permeate fluxes of nanoparticle membranes with respect to number of coats of (a) 120 nm (b) 300 nm sized particles at 10 bar and 27˚C in PS/toluene solution

Table 3 summarizes the membranes filtration performance in different solvents.

Table 3 Nanofiltration results in different solvents

Membrane code	Toluene		Acetone		% Flux decrease [a]
	Flux $Lm^{-2}h^{-1}$ 10bar/30bar	**MWCO $gmol^{-1}$**	**Flux $Lm^{-2}h^{-1}$ 30 bar**	**MWCO $gmol^{-1}$**	
M1	38/55	>> 1095	80	>>1095	30
M2	27/45	~550	72	~440	19
M3	21/35	~450	68	~360	18.5
M4	18/25	~340	44	~260	17
M5	15/35	> 1095	48	> 1095	16
M6	8/24	> 1095	40	> 1095	15
M7	4/15	~500	30	~500	14.5
M8	-/20	~220	40	~220	10
S122*	-/17	~270	.....	.....	51
Puramem* 280	-/20	~280	.....	.....	33
S380*	-/114	~495	.....	.....	12

* Note that the Starmem 122, Puramem 280 and S380 are not stable in acetone so a comparison cannot be undertaken.

[a] Calculated using Equation 4

3.2.4 Membrane flow properties – application of different models

Most of the models describing membrane transport assume the membranes is a porous medium, and a broad range of pore structures are possible such as cylindrical, irregular and interconnected pores. These structures define the flow properties of the membranes and are described by

different models. Formation of a nanoparticle layer on a porous polymer support results in an asymmetric composite structure (composite membrane). These composite membranes contain two distinct types of pores, large irregular pores in the polymer support and narrowly dispersed pores between the closely packed nanoparticles in the layer. The latter are assumed to determine the flow properties of the membrane. Dense packing of spherical nanoparticles is the most common and simple model system for flow through such porous media. For the general case of flow through porous medium Darcy's law states the permeability as a direct relationship between rates of flow and pressure gradient. Carman-Kozeny theory using this Darcy's law explains the flow through porous structures formed by packing of particles[34, 35].

The flow rate through a packed bed of closely packed spheres is given by the following equation

$$Q = \frac{A_f \rho_n \varepsilon^3 {D_n}^2 \Delta P}{M\eta 180(1-\varepsilon)} \quad (13)$$

Where η is the fluid viscosity, A_f is the area of the packed bed of length L, ρ_n is the density of nanoparticles, D_n is the diameter of nanoparticles, ΔP is the pressure difference across the membrane, M is the mass of latex particle per unit area and ε (~0.4) is the porosity of nanoparticle layer. Flux can be calculated by

$$J = \frac{Q}{A_f} \quad (14)$$

Carman-Kozeny correlates measured permeabilities with the internal surface area and solid volume fraction of porous medium and works in the laminar region where viscous forces are dominant[36-39]. This model explains the flow directly proportional to pressure drop and inversely proportional to fluid viscosity[40]. According to these equations the resistance to flow of a

nanoparticle layer can be controlled by the particle size and the thickness of the nanoparticle layer – a trend which is in agreement with our experimental results.

Another way to describe flow through a packed bed is to use equation established by Leva[35]. In this equation particles are considered smooth spheres, flow is laminar, and end effects are minimal. Applying this equation to a layer consisting of nanoparticles, the resistance can be calculated from its volume porosity ε, diameter of nanoparticles D_n, density of nanoparticles ρ_n and mass of nanoparticles applied per unit area M.

$$R = \frac{[200M\,(1-\varepsilon)]}{\rho_n D_n^2 \varepsilon^3} \quad (15)$$

Then flux through the membrane can be calculated by transmembrane pressure ΔP and viscosity η

$$J = \frac{\Delta P}{\eta R} \quad (16)$$

Table 4. Flux estimation using Carman-Kozeny and Leva's equations using toluene as solvent at 30bar

Membrane code	**Flux (Leva) m.h^{-1} b**	**Flux (Carman-Kozeny) m.h^{-1} a**	**Actual flux m.h^{-1}**
M2	0.036	0.321	0.045
M3	0.007	0.058	0.035
M4	0.003	0.023	0.025
M5	0.025	2.353	0.035
M6	0.031	0.294	0.024
M7	0.014	0.130	0.015

Table 5. Flux estimation using Carman-Kozeny and Leva's equations using acetone as solvent at 30bar

Membrane code	Flux (Leva) $m.h^{-1}$ [b]	Flux (Carman-Kozeny) $m.h^{-1}$ [a]	Actual flux $m.h^{-1}$
M2	0.036	0.184	0.072
M3	0.006	0.033	0.068
M4	0.003	0.013	0.044
M5	0.254	1.352	0.048
M6	0.031	0.169	0.040
M7	0.014	0.075	0.030

[a] calculated using equation 14, [b] calculated using equation 16

Results in Table 4 and Table 5 show that flux calculated via the Carman-Kozeny equation is relatively high as compared to actual membrane flux. Leva's equation predicted gives less deviation from the experimental flux values for 300nm sized nanoparticles but the flux predicted for 120nm sized nanoparticles is considerably lower than the experimental one.

There are two major factors behind this difference. One of the most important factors is the size of particles and pores. The Carman-Kozeny equation applies for the particles and pores in the range of >0.25 mm. The pore sizes expected in this study was in the range of 9 to 23nm as calculated by equation 17 suggested by Wood and Sourirajan[41].

$$\frac{r_n}{r_{int}} = 6.464 \qquad (17)$$

The rejection performance suggests pore size to be even smaller, possibly due to particle deformation as explained in section 3.2.3. Apparently the flow properties change with the size of pores.

The second major factor is the response of nanoparticle layers in organic solvents. The flow properties would also be affected by the degree of swelling of polymeric nanoparticles in different solvents and by the nanoparticle-solvent interaction. Thus the flow depends upon the packing material properties.

Both models failed to describe the flow behavior properly, most likely due to the fact that they are developed for rigid non-swelling particles and not in the nanosize range. Particle-solvent interaction can be expected to vary with solvent properties including molecular volume and Hildebrand solubility parameter[42]. The Hildebrand solubility parameter of acetone and toluene are 19.7 and 18.3 $MPa^{1/2}$ respectively. We calculated solubility parameter for P(NIPAM-HEMA) (the cross-linker was not taken into account) from the group contribution method as applied by Dunkel[43] of 22.5 $MPa^{1/2}$. This suggests that none of the above solvents would be a very "good" solvent for P(NIPAM-HEMA), however acetone would be a reasonable one. Thus the nanoparticles will swell more in acetone, allowing higher solvent penetration through the nanoparticle material. On the other hand increasing the degree of swelling of the nanoparticles will result in smaller interstitial spaces (smaller pores) thus decreasing the MWCO of membranes. Opposite effects will occur with toluene which is a "poor" solvent for P(NIPAM-HEMA) resulting in lower degree of swelling of the nanoparticles, reduced solvent penetration through particle material, larger interstitial spaces and higher MWCO. Furthermore the molar volume of toluene (106 $cm^3.mol^{-1}$) is one and half times higher than acetone (73.3 $cm^3.mol^{-1}$) and could also contribute to its lower permeation rate. Moreover, size and shape (hydrodynamic radius) of oligostyrenes in different solvents could also result in different MWCOs[44]. Some studies suggest that the surface tension of solvent and hydrophilicity/hydrophobicity of particle surface are also major factors determining the flux and rejection of membranes[42]. In addition the

cross-linking of the nanoparticles will also affect the membrane performance. In short, there are many factors which should be considered when describing the transport through OSN membranes and despite the extensive research in this area membrane transport is still not well understood. Detailed mathematical description and understanding of the transport properties of our membranes prepared from nanoparticles is beyond the scopes of this paper. Our intention is to demonstrate that this method for membrane preparation is a viable alternative to the currently used phase inversion technique, which allows for better control over the membrane structure and separation properties. Further extensive investigations using a variety of nanoparticles might lead to improved control over the membrane structure and performance.

4. Conclusion

A new class of OSN membranes has been created by coating an ultrafiltration support with nanoparticles of different diameters, and then subsequently crosslinking the particles to make the membrane stable during filtration with organic solvents. Using this technique membranes can be produced with a wide range of MWCO, and separation performance could be tuned by simply varying the size of the nanoparticles and thickness of the nanoparticles layer. Furthermore, a multilayered combination of nanoparticles of different sizes broadens even further the potential of this technique which we believe offers an exciting new opportunity for producing membranes with finely tunable separation properties.

5. Acknowledgement

The authors wish to acknowledge University of Engineering and Technology Lahore Pakistan and FP7 GA-CP-FP 214095-2 HiCat project for financial assistance. Mrs Aleka Manousaki is acknowledged for her assistance in microgel imaging by SEM. We also thank Mr. Andreas Pamvouxoglou for his help with the DLS measurements.

Nomenclature

A_f Area of packed bed (cm^2)

A_m Area of membrane (cm^2)

A_n Cross sectional area of one nanoparticle (cm^2)

C_{Fi} Concentration of styrene oligomer in retentate (-)

C_{Pi} Concentration of styrene oligomer in permeate (-)

D_n Diameter of nanoparticle (cm)

J Flux through the membrane ($L.m^{-2}.h^{-1}$)

L_n Total number of nanoparticle layers coated on membrane (-)

M Mass of latex per unit area ($g.cm^{-2}$)

N_n Total number of nanoparticle in one layer (-)

ΔP Transmembrane pressure (Pa)

Q Flow rate through packed bed of nanoparticles ($cm^3.s^{-1}$)

R Resistance (cm^{-1})

r_{int} Void radius (cm)

r_n Radius of nanoparticle (cm)

V Volume of nanoparticle coated on the membrane (cm^3)

V_n Volume of one nanoparticle (cm^3)

ρ_n Density of nanoparticles ($g.cm^{-3}$)

ε Porosity of bed (-) (value was taken from F.A.L. Dullien, "Porous Media. Fluid Transport and Pore Structure", 2nd edition, Academic Press Inc, 1992 for regular closely packed sphere

η Viscocity of fluid (Pa.s) (for acetone and toluene taken from Perry's hand book for chemical engineers 6^{th} edition at 300K)

References

(1) Baker, R. W. Future Direction of Membrane Gas Separation Technology, *Ind. Eng. Chem. Res.* **2002**, 41, 1393.

(2) Vandezande, P.; Gevers, L. E. M.; Vankelecom, I. F. J. Solvent Resistant Nanofiltration: Separating on a Molecular Level. *Chem. Soc. Rev.* **2008**, 37, 365.

(3) Wong, H. T.; Pink, C. J.; Ferreira, F. C.; Livingston, A. G. Recovery and Reuse of Ionic Liquids and Palladium Catalyst for Suzuki Reactions Using Organic Solvent Nanofiltration. *Green Chem.* **2006**, 8, 373.

(4) Wong, H. T.; See-Toh, Y. H.; Ferreira, F. C.; Crook, R.; Livingston, A. G. Organic Solvent Nanofiltration in Asymmetric Hydrogenation: Enhancement of Enantioselectivity and Catalyst Stability by Ionic Liquids. *Chem. Commun.* **2006**, 19, 2063.

(5) Han, S.; Wong, H. T.; Livingston, A. G. Application of Organic Solvent Nanofiltration to Separation of Ionic Liquids and Products from Ionic Liquid Mediated Reactions. *Chem. Eng. Res. Des.* **2005**, 83, 309.

(6) See-Toh, Y. H.; Lim, F. W.; Livingston, A. G. Polymeric Membranes for Nanofiltration in Polar Aprotic Solvents. *J. Membr. Sci.* **2007**, 301, 3.

(7) Wei, W.; Xiangli, F. J.; Jin, W. Q.; Xu, N.P. Solvent Resistant Nanofiltration Membranes. *Prog. Chem. 2007*, 19, 1592.

(8) See-Toh, Y. H.; Silva, M.; Livingston, A. G. Controlling Molecular Weight Cut-off Curves for Highly Solvent Stable Organic Solvent Nanofiltration (OSN) Membranes. *J. Membr. Sci.* **2008**, 324, 220.

(9) Mähr, U.; Purnama, H.; Kempin, E.; Schomäcker, R.; Reichert, K. H. Synthesis and Characterization of Porous Polymer Membranes Produced by Interparticle Crosslinking. *J. Membr. Sci.* **2000**, 171, 285.

(10) Dauben, M.; Reichert, K. H.; Huang, P.; Fock, J. Preparation of Polymeric Porous Materials by Interparticle Cross-linking. *Polymer. 1996*, 37, 2927.

(11) Jons, S.; Ries, P.; McDonald, C. J. Porous Latex Composite Membranes: Fabrication and Properties. *J. Membr. Sci.* **1999**, 155, 79.

(12) Ramakrishnan, S.; McDonald, C. J.; Prudhomme, R. K.; Carbeck, J. D. Latex Composite Membranes: Structure and Properties of the Discriminating Layer. *J. Membr. Sci.* **2004**, 231, 57.

(13) Lehmann, M.; Brunner, H.; Tovar, G. E. M. Selective Separations and Hydrodynamic Studies: a New Approach Using Molecularly Imprinted Nanosphere Composite Membranes. *Desalination.* **2002**, 149, 315.

(14) Lehmann, M.; Brunner, H.; Tovar, G. E. M. Molecularly Imprinted Nanoparticles as Selective Phase in Composite Membranes: Hydrodynamics and Separation in Nanoscale Beds. *Chem. Ing. Tech.* **2003**, 75, 149.

(15) Sára, M.; Pum, D.; Sleytr, U. B. Permeability and charge-dependent adsorption properties of the S-layer lattice from Bacillus coagulans E38-66. J. *Bacteriol.* **1992**, 174, 3487.

(16) Sidhu, M. S.; Olsen, I. S-layers of Bacillus species. *Microbiology.* **1997**, 143, 1039.

(17) Pum, D.; M. Sara,; U. B. Sleytr. Structure, surface charge and self-assembly of the S-layer lattice from Bacillus coagulans E38-66. *J. Bacteriol.* **1989**, 171, 5296.

(18) Sira, M.; Sleytr, U. B. Production and characteristics of ultrafiltration membranes with uniform pores from twodimensional arrays of proteins. *J. Membr. Sci.* **1987**, 33:27.

(19) Park, C.; Yoon, J.; Thomasb, E. L. Enabling nanotechnology with self-assembled block copolymer patterns. *Polymer.* **2003**, 44, 6725.

(20) Hashimoto, T.; Tsutsumi, K.; Funaki, Y. Nanoprocessing based on bicontinuous microdomains of block copolymers: Nanochannels coated with metals. *Langmuir*. **1997**, 13, 6869.

(21) Jonquieres, A.; Clement, R.; Lochon, P. Permeability of block copolymers to vapors and liquids. *Prog. Polym. Sci.* **2002**, 27, 1803.

(22) Xiang, H.; Shin, K.; Kim, T.; Moon, S.; Mccarthy, T. J.; Russell, T. P. The Influence of confinement and curvature on the morphology of block copolymers. *J. Polym. Sci.* **2005**, 43, 3377

(23) See Toh, Y. H.; Loh, X. X.; Li, K. Bismarck A.; Livingston, A.G. In search of a standard method for the characterization of organic solvent nanofiltration membranes. *J. Membr. Sci.* **2007**, 291, 120.

(24) Mathworld.wolfram.com/CirclePacking

(25) Conway, J. H; Sloane, N. J. A. *Sphere Packings, Lattices and Groups*; Springer Verlag: New York, 1993.

(26) Cho, S. H.; Lim, H. S.; Jeong, B. K. *et al.* Thermally Stable Photoreactive Polymers as a Color Filter Resist Bearing Acrylate and Cinnamate Double Bonds. *Macromolecular Research*. **2008**, 16 (1), 31.

(27) Lee, T. Y.; Roper, T. M.; Jonsson, E. S. *et al.* The kinetics of vinyl acrylate photopolymerization. *Polymer*. **2003**, 44, 2859.

(28) Lee, T. Y.; Cramer, N.; Hoyle, C.; Stansbury, J.; Bowman, C. (Meth)Acrylate Vinyl Ester Hybrid Polymerizations. *J. Polym. Sci. A Polym. Chem.* **2009** , 47, 2509.

(29) Sperry, P. R.; Snyder, B. S.; O'Dowd, M. L.; Lesko, P. M. Role of water in particle deformation and compaction in latex film formation. *Langmuir.* **1994**, 10, 2619.

(30) Stewarda, P.A.; Hearna, J.; Wilkinsonb, M. C. An overview of polymer latex film formation and properties. *Adv. Colloid. Int. Sci.* **2000**, 86, 195.

(31) Routh, A. F.; and Russel, W. B. Deformation mechanisms during latex film formation: Experimental evidence. *Ind. Eng. Chem. Res.* **2001**, *40*, 4302.

(32) Sarah, T.; Eckersley.; Rudin, A. Film formation of acrylic latexes. A comprehensive model of film coalescence. *J. App. Polym. Sci.* **1994**, 53, 1139.

(33) Schild, H. G. Poly(N-isopropylacrylamide):experiment, theory and application. *Prog. Polym. Sci.,* **1992**, 17, 163.

(34) Leva, M. Fluid Flow through Packed Beds. *Chem. Eng.* **1949**, 56, 115.

(35) Davis, R.; Grant, D.; *Theory of Dead End Nanofiltration; Membrane Handbook*; Van Nostrand Reinhold: New York, 1992.

(36) Philipse, A.; Pathmamanoharan, C. Liquid Permeation (and Sedimentation) of Dense Colloidal Hard Sphere Packings. *J. Colloid. Interf. Sci.* **1993**, 159, 96.

(37) Carman, P. C. *Flow of Gases through Porous Media*; Academic Press: New York, 1956.

(38) Scheidegger, A. *Physics of Flow through Porous Media*; University of Toronto Press: Canada, 1974.

(39) Schere, G.; Swiatek, R. Measurement of Permeability II. Silica Gel. *J. Non-Cryst. Solids.* **1989**, 113, 119.

(40). Warren, M.; Smith, L.; Harriot, C. *Unit Operations of Chemical Engineering*; McGraw-Hill: New York, 2005.

(41) Wood, H.; Sourirajan, S. The Effect of Polymer Solution Composition and Film-forming Procedure on Aromatic Polyamide Membrane Skin Layer Structure. *J. Colloid. Interf. Sci.* **1992**, 149, 105.

(42) Machado, D. R.; Hasson, D.; Semiat, R. Effect of solvent properties on permeate flow through nanofiltration membranes. *J. Membr. Sci.* **1999**, 163, 93.

(43) Miller-Chou, B. A.; Koenig, J. L. A review of polymer dissolution. *Prog. Polym. Sci.* **2003**, 28, 1223.

(44) Beerlage, M. A. M. Polyimide membranes for non-aqueous systems, *Thesis, University Twente*, 1994